Optical Engineering

OpticalEngineering.SPIEDigitalLibrary.org

Pseudorandom orbiting stroke for freeform optics postprocessing

Xiangyu Guo
Yong Shu
Geon-Hee Kim
Michael Palmer
Heejoo Choi
Dae Wook Kim

SPIE.

Xiangyu Guo, Yong Shu, Geon-Hee Kim, Michael Palmer, Heejoo Choi, Dae Wook Kim, "Pseudorandom orbiting stroke for freeform optics postprocessing," *Opt. Eng.* **58**(9), 092608 (2019), doi: 10.1117/1.OE.58.9.092608.

Downloaded From: https://www.spiedigitallibrary.org/journals/Optical-Engineering on 06 Nov 2019
Terms of Use: https://www.spiedigitallibrary.org/terms-of-use

Pseudorandom orbiting stroke for freeform optics postprocessing

Xiangyu Guo,[a] Yong Shu,[b] Geon-Hee Kim,[c] Michael Palmer,[a] Heejoo Choi,[a] and Dae Wook Kim[a,d,*]
[a]University of Arizona, James C. Wyant College of Optical Sciences, Tucson, Arizona, United States
[b]Air Force Engineering University, Aviation Maintenance NCO Academy, Xinyang, China
[c]Korea Basic Science Institute, Ultra-Precision Engineering Laboratory, Daejeon, Republic of Korea
[d]University of Arizona, Department of Astronomy and Steward Observatory, Tucson, Arizona, United States

Abstract. In addition to achieving a desired freeform profile, ensuring a superb micro-roughness finish is a key factor for successful freeform optics manufacturing. We present a pseudorandom orbiting stroke-based postprocessing technique that maintains freeform optic forms, while improving small-scale surface quality. The full-aperture tool can avoid subaperture effects, and the small stroke pseudorandom tool path guarantees the match of freeform profiles while preventing the directionality of the final surface profiles. Three independent experimental studies are designed, conducted, and presented for a wide range of optics, including magnetorheological finishing-polished BK7 glass, single-point diamond turned (SPDT) poly(methyl methacrylate), and SPDT Al6061 optics. The comparison of direct measured maps on the initial and final smoothed optics verifies the form maintenance capability of the freeform optics postprocessing technology. Surface roughness measurement highlights improvements in local surface roughness and periodic toolmark errors left by the previous polishing method. © *2019 Society of Photo-Optical Instrumentation Engineers (SPIE)* [DOI: 10.1117/1.OE.58.9.092608]

Keywords: freeform optics; postprocessing; smoothing; surface roughness; pseudorandom orbiting stroke.

Paper 190075SS received Jan. 18, 2019; accepted for publication Apr. 2, 2019; published online Apr. 17, 2019.

1 Introduction

One significant characteristic of freeform optics is that the local radius of curvature varies across the surface. Thus, imperfect matching between the tool and the optical surface under fabrication will cause nonuniform pressure distribution and lead to local or zonal surface figure errors. Although opticians often prefer large rigid tools, which induce fewer small-scale errors, to accommodate the locally varying aspheric/freeform optics and to correct localized surface errors more rapidly, they utilize small tools with a computer-controlled tool path to fabricate such nonspherical optics.[1,2] However, due to the uncertainties in the material removal rate and regular tool path, the subaperture figuring process using a small tool can generate mid-to-high spatial frequency errors on the surface. Apart from that, a more adaptable method known as single-point diamond turning (SPDT) has been developed and widely used by the precision optical manufacturing community since the 1970s,[3] especially for soft ductile materials. The existence of mid-to-high spatial frequency errors continues to be a problem.

To overcome the weakness of the traditional subaperture polishing tool, Kim and Burge[4] proposed a rigid conformal tool, which combined a non-Newtonian fluid with traditional polishing pads to obtain a balance between freeform conformability and smoothing rigidity. Another noteworthy development concerns the field of tool path control and optimization. To restrain small tool footprint marks and to minimize the mid-to-high spatial frequency errors, new tool paths are applied to replace regular raster and spiral paths. Zeeko Ltd.'s "precessions"[5] developed the unicursal path, and Tam et al.[6] presented peano-like paths in 2013. Finishing processes such as ion beam figuring (IBF)[7] and magnetorheological finishing (MRF)[8] are also used. Even though the well-controlled IBF and MRF may not generate mid-to-high spatial frequency errors, another smoothing process is often required to achieve better surface quality.

A postsmoothing process can be applied to further decrease the mid-to-high spatial frequency errors, while achieving the desired freeform surface figure and better surface quality conveniently. OPTIMAX invented and matured a proprietary VIBE™ technology,[9] which is a full-aperture high-speed computer-controlled surface smoothing process. This technology has been successfully applied and demonstrated to rapidly postsmooth aspherical or freeform optics with a high surface quality, but the technical details have not been reported due to its proprietary nature as a key technology of OPTIMAX.

Inspired by the VIBE approach, and aiming at both maintaining the desired freeform optical surface figure and decreasing the high spatial frequency surface errors (i.e., surface roughness) for various optical materials and freeform manufacturing methods, we developed a pseudorandom orbiting stroke (PROS) computer numerical control (CNC) postprocessing technique, which can be applied to varied optics sizes, materials, and prepolishing methods. Three representative experimental case studies using freeform optics made out of glass (BK7), plastic [Poly(methyl methacrylate) or PMMA], and aluminum (Al6061) for diameters ranging from 30 to 100 mm are presented to prove the performance of the proposed postprocessing technique.

*Address all correspondence to Dae Wook Kim, E-mail: letter2dwk@hotmail.com

0091-3286/2019/$28.00 © 2019 SPIE

Downloaded From: https://www.spiedigitallibrary.org/journals/Optical-Engineering on 06 Nov 2019
Terms of Use: https://www.spiedigitallibrary.org/terms-of-use

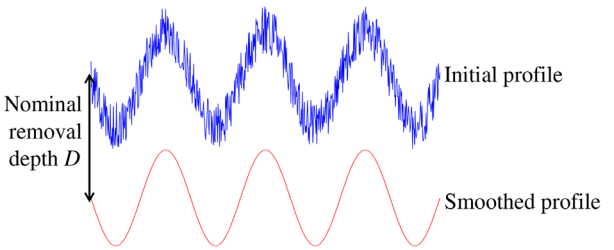

Fig. 1 Ideal postprocessing using PROS process, which removes a uniform layer of materials (i.e., nominal removal depth), while maintaining the original surface profile and improves the high spatial frequency surface finish.

2 Pseudorandom Orbiting Stroke Postprocessing Technique

An ideal smoothing process should keep the original freeform surface profile, while improving the local surface roughness quality. The goal of the PROS technique is the same. With the characteristic of the full-aperture smoothing, the expected removal depth across the entire aperture of the optics should be uniform. The schematic of the PROS postprocessing effect is presented in Fig. 1.

According to Preston's law, the nominal removal depth (D) is predicted as

$$D = \mathrm{K}_{\mathrm{preston}} \cdot P \cdot V \cdot t, \tag{1}$$

where K_{preston}, P, V, and t are the four parameters representing Preston's constant (i.e., removal rate), polishing pressure, relative velocity between the tool and the optics, and dwell time, respectively.[10] Thus, critical factors that should be monitored to achieve a uniform removal depth in PROS CNC postprocessing are maintenance of a stable slurry application, uniform distribution of polishing pressure, and random distribution of the velocity vectors (speed and direction) along the smoothing path between the tool and the optical surface.

2.1 *Fabrication Parameters*

The tool and slurry choices are important aspects governing Preston's constant. A pitch lap tool is often made to match the form of optics due to its viscoelastic property.[11] To achieve better matching and proper hardness of the pitch lap tool, we use the combination of Gugolz #64 and #73 pitches. Aluminum or brass plates with a centered hole are chosen as the base of the pitch tools. The tool size is selected to be the same as the size of the workpiece, and the shape of the pitch lap must take the exact shape of the desired optic. Otherwise, the optical surface profile will be changed.[12] To obtain the same optics shape, the pitch tool is pressed on the sample, as shown in Fig. 2.

Apart from the pitch, polishing pads such as the polyurethane pad and napped porometric polymer pad are also chosen depending on the material and surface quality of the samples. The choices of smoothing slurry for each sample are discussed in Sec. 3.

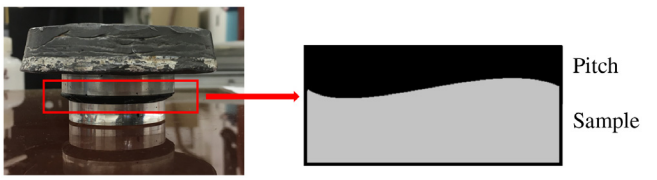

Fig. 2 Tool pressing process.

2.2 *Small Stroke Computer Numerical Control Pseudorandom Orbiting Stroke*

It is difficult to adapt the asymmetric surface shape and matching of the tool and optics with large stroke motion, especially for smoothing freeform optics. Thus, we apply the small orbital stroke motion for the postprocessing process, allowing pitch flow and continuous conforming to the shape[10] simultaneously.

The regular tool path will contribute to the systematic misfit between the tool and the workpiece, which will lead to directionality of the surface profile in the final product. Even with small stroke motion, a smooth path with directionality is impossible to maintain in the original surface profile. A full-aperture small-stroke directional experiment on a SPDT PMMA material is implemented to experimentally prove and confirm the undesired directional characteristic in the surface profile. The tool stroke pattern follows a 2-mm horizontal (x direction) linear motion, and the surface freeform pattern for the SPDT surface is spiral. The top view of the experiment setup as well as the smoothing parameters are described in Fig. 3, where d stands for the stroke distance.

We compare the smoothing effect in two profiles (shown in Fig. 3) of this PMMA sample, which are measured by the white light interferometer. The first concerns the smoothing direction along the diamond-turned pattern (blue line in area A), and the second against the diamond-turned pattern (red line in area B). The direct measured initial and smoothed surface profiles as well as power spectral density (PSD) comparison for each smoothing process are shown in Fig. 4.

The corresponding microsurface roughness value and varied ratio of the initial and smoothed states are presented in Table 1.

Note that the against smoothing direction result shows that the roughness parameters, namely the peak-to-valley (PV) and average roughness (Ra), decrease by about 20% and 10%, and the PSD for the high spatial frequency also improves, as shown in Fig. 4, which can be observed in the red circled area. However, the along smoothing direction result does not show much variation. Therefore, the smoothing

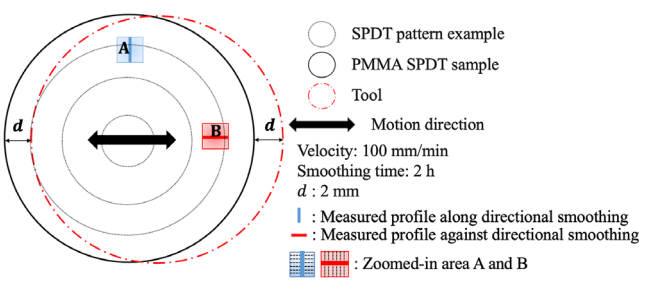

Fig. 3 Top view of the directional smoothing experimental setup.

Downloaded From: https://www.spiedigitallibrary.org/journals/Optical-Engineering on 06 Nov 2019
Terms of Use: https://www.spiedigitallibrary.org/terms-of-use

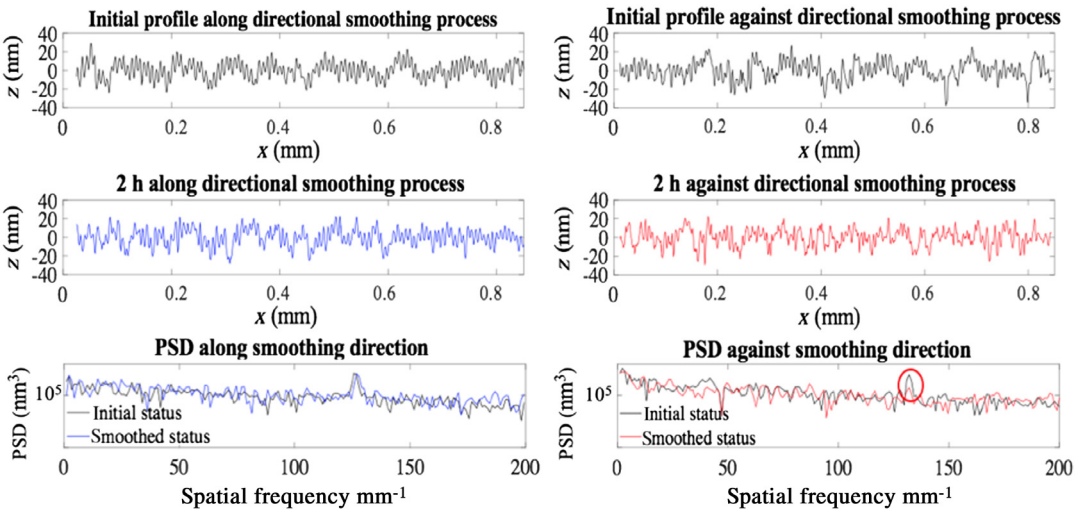

Fig. 4 Surface profile comparison: (a) PSD against and (b) along the directional smoothing process.

Table 1 Roughness parameters PV and Ra for each surface profile in each smoothing process.

	Measured profile direction in Fig. 3	Initial state	Smoothed state	Varied ratio (%)
PV (nm)	Against (red line)	64.82	51.88	19.96
Ra (nm)		8.10	7.20	11.11
PV (nm)	Along (blue line)	53.61	50.97	4.92
Ra (nm)		7.47	7.50	0.4

direction affects the smoothing result considerably. The high spatial frequency errors can only be removed if the smoothing direction is always opposite to the direction of error. Thus, to achieve global smoothing effect, the direction of the smoothing process should be randomly distributed in every direction.

Accordingly, we set our smoothing path as a PROS pattern, in which the ending position coincides with the beginning position. To operate such a smoothing path, G-Code language is applied and a MATLAB-based data-processing module is developed. As the pin connects the center of the tool and the CNC machine, the position of the smoothing path is related to the tool's center position.

The beginning position is defined by the parameter named "offset" (mm) in this module; the initial offsets for x and y are 0, which means that the center of the tool coincides with the center of the workpiece. We use the polar coordinate system for setting up the parameters for the orbital stroke. The largest orbital radius of each stroke of the PROS tool path is defined as $r_{\max}$. To achieve uniform removal depth, during the PROS process, each stroke radius and the velocity are randomly selected within the range of given $r_{\max}$ (mm) and the maximum feed rate (mm/min). At the same time, the angular direction of each PROS circular path is randomly distributed in order to ensure the pseudorandom characteristic of the stroke. The uniform random distribution is used in the PROS path generation. The running time (min) in the module roughly defines how many circular patterns will exist during the whole smoothing process.

Figure 5 shows the relationship among the largest radius $r_{\max}$, the PROS tool path, and the smoothing area. The black solid, red dash-dotted, and blue dashed circles represent the workpiece, tool, and PROS tool path, respectively. In Fig. 5(a), the red o denotes the beginning point; here, c_1 and c_2 are the two example positions of the tool center during the PROS postprocessing with the largest radius $r_{\max}$, and the blue shaded area is the uniform smoothing area or the area where the tool always contacts the workpiece. Figure 5(b) shows an example of the PROS tool path, which is determined by the user-defined inputs for the tool path-generating module.[13]

When the sizes of the tool and workpiece are the same, the uniform smoothing area cannot cover the whole workpiece. We set the radius of workpiece as R, so that the ratio between the uniform smoothed area and the workpiece area E is given as

$$E = \frac{(R - 2r_{\max})^2}{R^2} \times 100\%. \tag{2}$$

As seen later (Table 2), the workpiece size or smoothed area is the uniform smoothed area, and the measured diameter corresponds to the effective diameter.

2.3 *Computer Numerical Control Machine Configuration*

The CNC schematic setup is presented in Fig. 6. The workpiece is fixed by two clamps and one fixed screw along the circumferential direction. The tool is driven by a pin to provide the degree of freedom for linear motion in the x and y directions as well as rotating motion, and lubricant is added to the connection area to ensure free rotation. Pressure is loaded by attaching an extra uniform weight. The centers of both the tool and the workpiece coincide at the beginning and finishing positions.

Downloaded From: https://www.spiedigitallibrary.org/journals/Optical-Engineering on 06 Nov 2019
Terms of Use: https://www.spiedigitallibrary.org/terms-of-use

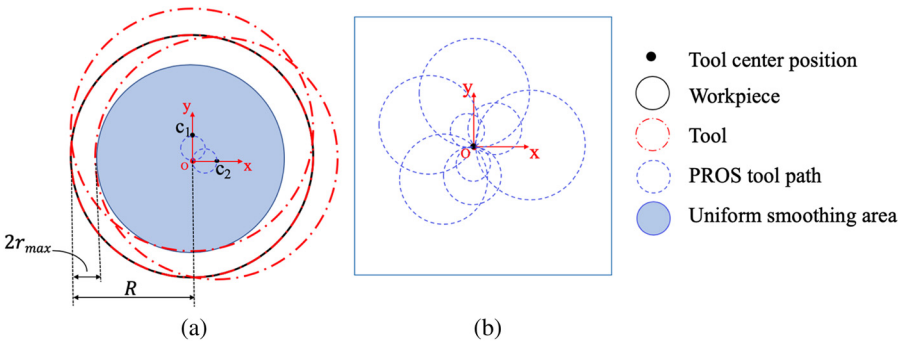

Fig. 5 Schematic representation showing the geometrical relationship between the workpiece and (a) the tool and (b) the PROS tool path generated using the CNC machine control software.

Table 2 Description of the initial states of the BK7, PMMA, and Al6061 workpieces.

	BK7	PMMA	Al6061
Prepolishing method	MRF	SPDT	SPDT
Freeform profile	Spiral	Trefoil	Astigmatism
Diameter (mm)	100	30	50.8
Effective diameter (mm)	96.4	28	44
Radius of curvature (mm)	136.8	120	∞
Central obscuration ratio	0.20	0	0.33

Table 3 Postprocessing information of the BK7, PMMA, and Al6061 workpieces.

	BK7	PMMA	Al6061
Maximum feed rate (mm/min)	100	100	100
Maximum radius r_{max} (mm)	1	1	1
Pressure (psi)	0.3	0.3	0.1
Pitch type	Combination of #64 pitch and #73 pitch (common)		
Pad type	—	LP-66 pad	Black CHEM2 pad
Solution	Water	Water	Olive oil
Postprocessing compound	Rhodite 906	Rhodite 906	S1: 50 nm alumina
			S2: —
Running time (min)	40	105	S1: 600
			S2: 90

3 Experimental Setup and Metrology Configuration

3.1 *Pseudorandom Orbiting Stroke Postprocessing Experimental Setup*

Three representative experimental cases are discussed in this section, each with a different optics material, prepolishing method, and surface shape. The initial-state descriptions of all workpieces are listed in Table 2, and the basic postprocessing information appears in Table 3.

As listed in Table 3, the postprocessing tool for workpiece BK7 is a pitch tool, and pads are chosen and joined to the pitch tool for PMMA and Al6061. LP-66 is a cerium oxide-filled polyurethane pad and the black CHEM2 pad is a porometric polymer pad with a consistency similar to a rubber-type pad. It behaves as an intermediate polishing pad, showing performance between those of low-napped and high-napped pads.[14] Unlike the postprocessing for the BK7 and PMMA samples, two stages exist in the case of the Al6061 sample. The first stage lasts 600 min with 50-nm alumina compound mixed with olive oil, and the second stage lasts 90 min with pure olive oil.

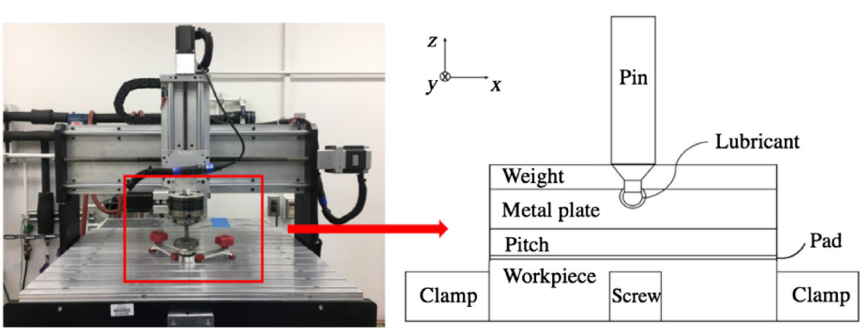

Fig. 6 Schematic representation of the PROS process CNC setup.

Downloaded From: https://www.spiedigitallibrary.org/journals/Optical-Engineering on 06 Nov 2019
Terms of Use: https://www.spiedigitallibrary.org/terms-of-use

3.2 *Measurement Configuration for Data Acquisition*

A VeriFire™ interferometer (ZYGO) is used for analyzing the full-aperture surface map. The results of directly measured initial and smoothed surface maps will support the maintenance of the surface profile. A NewView™ 800 white light interferometer (ZYGO) is used for analyzing the microsurface roughness condition, and we choose Ra, the arithmetical mean deviation, to present the results. The specific measurement parameter settings are listed in Table 4.

The same square-shaped location measurement pattern is set for the whole surface. The micro-surface roughness result of each smoothing phase is given by the average Ra value of all measurements. Table 5 describes the measurement setup parameters and measurement patterns for three experiments.

Table 4 Measurement setup parameters for the white light interferometer.

Measurement setup	Settings
Objective lens	10× Mirau NA 0.3
FOV (mm)	0.83×0.83
Lateral resolution (micron)	0.815
Number of averaged measurements	3

Table 5 Micro-surface roughness measurement patterns for three experiments.

	BK7	PMMA	Al6061
Pattern area (mm^2)	64	25	36
Point spacing (mm)	1	0.625	0.75
Number of sampling points	9×9	9×9	9×9

4 Freeform Optics Postprocessing Performance

The postprocessing running time and final surface quality are determined by the material characteristics and initial surface quality. Notably, the final smoothed state of all the experiment samples shows good full-aperture surface freeform shape maintenance as well as improvements in surface quality.

In the presented experimental case study, the freeform optical samples are regarded as ideal (i.e., meeting the design tolerance) samples except for their microsurface roughness. The goal of this case study is to demonstrate the PROS postprocessing technique while keeping the as-manufactured freeform surface profiles.

4.1 *Surface Form Preservation Analysis*

Figure 7 presents the measured initial and smoothed maps as well as the subtracted maps for each workpiece. Table 2 provides more details of the sample surfaces, including the effective diameters for each case.

The smoothed surface maps are almost the same as the initial surface maps, which represent the as-manufactured ideal (i.e., meeting the design requirement and shape tolerance except for microsurface roughness) shape that needs to be maintained. Focusing on the subtracted surface map,

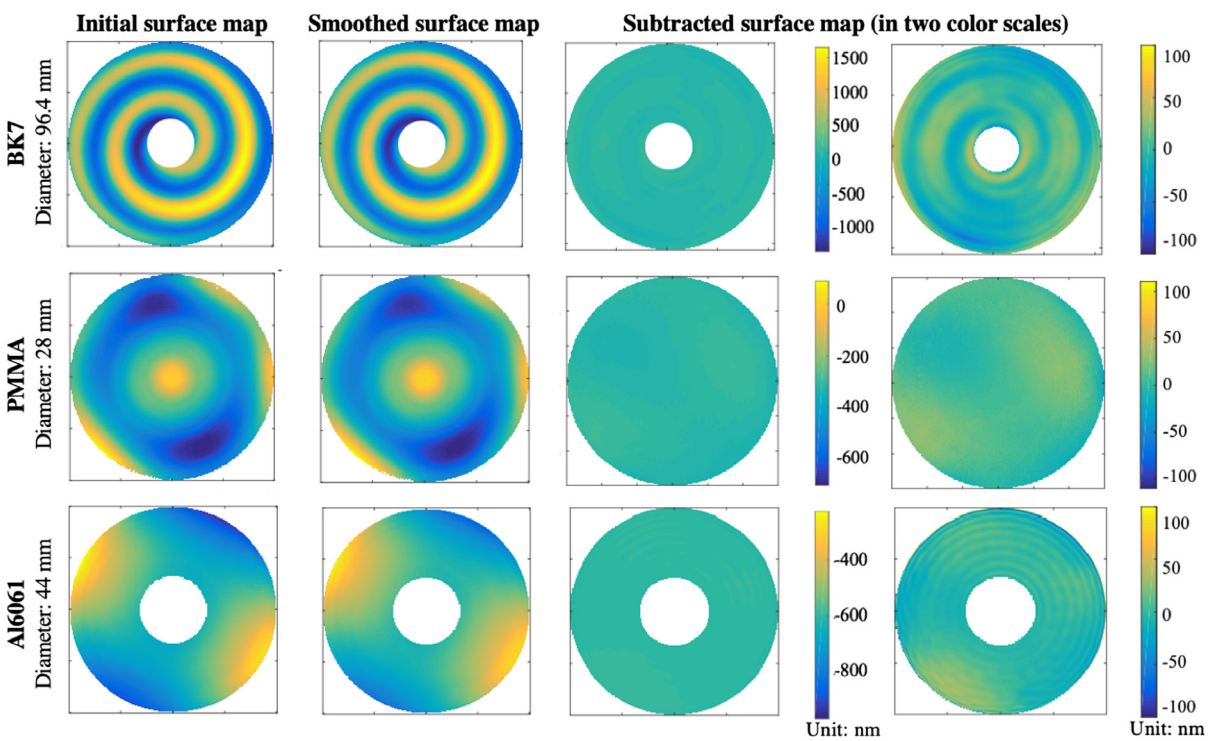

Fig. 7 Measured full-aperture surface maps using VeriFire™ interferometer for the initial and smoothed stages, and the corresponding subtracted surface map showing the difference before and after the PROS process.

Downloaded From: https://www.spiedigitallibrary.org/journals/Optical-Engineering on 06 Nov 2019
Terms of Use: https://www.spiedigitallibrary.org/terms-of-use

Table 6 Full-aperture PV and RMS comparisons of the initial, smoothed, and subtracted maps for BK7, PMMA, and Al6061 (Note: The "Initial map" represents the as-fabricated ideal freeform shape that needs to be preserved after the postprocessing.)

	Materials	Initial map	Smoothed map	Subtracted map	Varied ratio (%)
PV (nm)	BK7	3216.32	3125.76	442.05	13.74
RMS (nm)		804.76	801.16	33.65	4.18
PV (nm)	PMMA	2552.23	2196.70	298.55	11.69
RMS (nm)		481.74	421.68	23.99	4.98
PV (nm)	Al6061	1838.43	1794.04	266.54	14.47
RMS (nm)		276.54	250.54	13.52	4.89

which indicates the criterion for full-aperture freeform surface maintenance, the full-aperture root-mean-square (RMS) value is about 0.05λ (assuming $\lambda = 633$ nm), and the varied ratio of the initial and smoothed states is within 5%. The corresponding full-aperture PV and RMS comparisons are summarized in Table 6. It is important to note that the "initial map" in Table 6 represents the ideal freeform shape that needs to be preserved after the postprocessing. Thus, the purpose of this table is to verify a small "varied ratio" value regardless of its sign. Targeting a certain absolute value of the RMS (e.g., target design value) or decreasing the RMS value by smoothing is not the goal.

4.2 *Analysis of Microsurface Roughness Improvement*

After the postprocessing, an improvement in the microsurface roughness is evident for all workpieces, as illustrated in Fig. 8. The postprocessing run time for the intermediate and final states for each sample is provided in Table 7.

The microsurface roughness decreases with postprocessing time, and the decreased ratios from the initial to the final state for BK7, PMMA, and Al6061 are 78.93%, 46.49%, and 31.48%, respectively. The smoothed value depends on the original surface quality.

Moreover, a change in the statistical microsurface roughness (Ra) distribution is observed when tracking the result of each measured sampling point. We set the histogram Ra binning range as 1 nm. Figure 9 describes the statistical

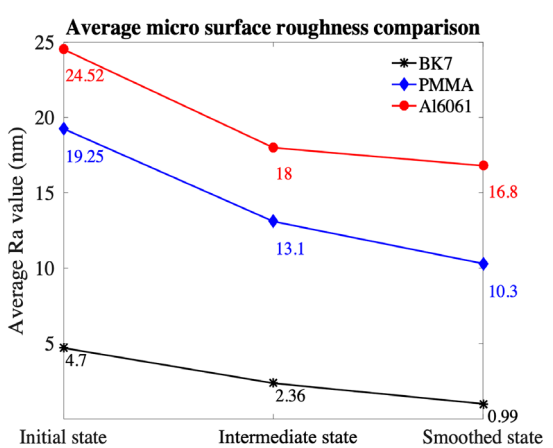

Fig. 8 Microsurface roughness comparison of all samples.

Table 7 Postprocessing times for each stage for BK7, PMMA, and Al6061.

	BK7	PMMA	Al6061
Intermediate state (min)	10	45	540
Final state (min)	40	105	690

distribution of measured microsurface roughness (Ra) as the PROS postprocessing is applied.

The initial distribution state depends on the previous polishing methods (e.g., MRF and SPDT). For each smoothed state, the Ra value increases and the peak value of the fitted curve moves to the left smaller Ra values as a result.

On a microscopic scale, the improvement in surface roughness and high spatial frequency errors are obvious. Considering that BK7 is polished using MRF, and the high spatial frequency errors are well controlled, we focus this discussion on the SPDT PMMA and Al6061 workpieces. Comparing the same measured areas, the toolmarks from SPDT gradually disappear. Choosing a line across the diamond-turned pattern of the surface map and analyzing the PSD as shown in Fig. 10, we note that the high spatial frequency errors are eliminated as a result of the PROS process.

The circled peak in the initial state is successfully decreased or eliminated in the final state, and, thus, the single measurement profiles are smoother after the PROS postprocessing. The clear suppression of the diffraction phenomenon from the previous SPDT process can also be observed visually. An example of the Al6061 workpiece is presented in Fig. 11.

The figure to the left shows the sample before the postprocessing process. The reflected image is clear and a significant diffraction phenomenon exists, which is caused by the periodic toolmarks. The figure to the right is the final smoothed sample, and we note that the diffraction phenomenon disappears and the reflected image is clearer, meaning there is less scattering and diffraction.

Thus, we can conclude that the PROS CNC-based postprocessing technique can maintain full-aperture profiles for freeform optics, while improving the surface quality; the finished samples exhibit lower microsurface roughness and fewer toolmarks.

Downloaded From: https://www.spiedigitallibrary.org/journals/Optical-Engineering on 06 Nov 2019
Terms of Use: https://www.spiedigitallibrary.org/terms-of-use

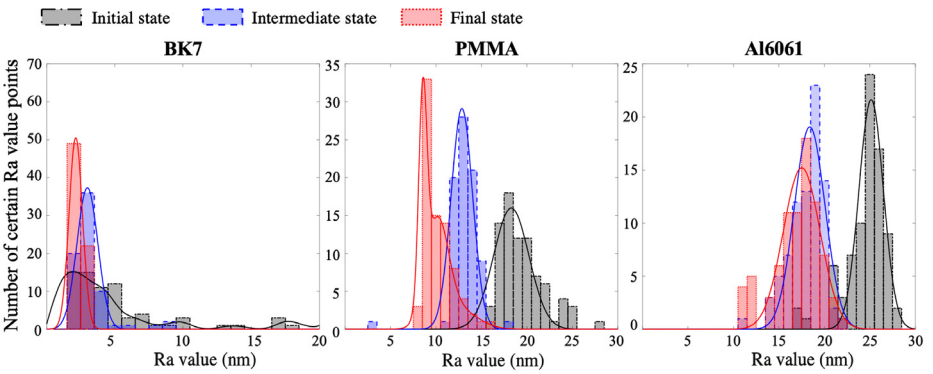

Fig. 9 Distribution of measured microsurface roughness (Ra) against various PROS postprocessing states. The bars and curves stand for the microsurface roughness distribution and fitted curve in each state, respectively.

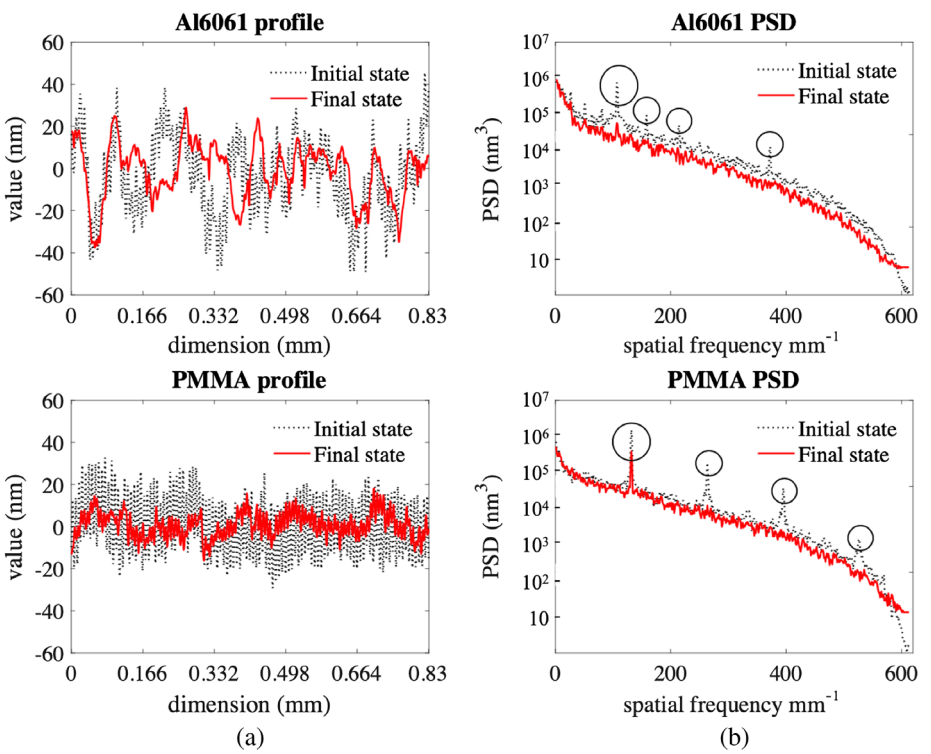

Fig. 10 Analyses of (a) linear profile data and (b) PSD for the SPDT PMMA and Al6061 samples before and after the PROS postprocessing.

Fig. 11 Visual appearance of the Al6061 sample (a) before and (b) after the smoothing process.

5 Conclusion

Modern freeform optics manufacturing is usually based on deterministic subaperture methods, and even though the desired surface form can be achieved, higher microsurface roughness and fewer high spatial frequency errors still pose barriers to a successful manufacturing process. The PROS CNC-based postprocessing technique presented in this paper is capable of maintaining the original correct surface form, while improving small-scale surface quality, and thus, it provides a convenient solution in freeform optics for different materials and apertures.

Three detailed independent experiments using different workpieces and finishing techniques, namely, BK7 (MRF), PMMA (SPDT), and Al6061 (SPDT), with distinctive surfaces are presented in this paper. Choices for slurries and parameter setup during the postprocessing are also listed and specified in detail to provide the authors a retraceability of the presented experimental data, which are very critical information as a fabrication research report. The varied ratio of the initial and smoothed states in the full-aperture

Downloaded From: https://www.spiedigitallibrary.org/journals/Optical-Engineering on 06 Nov 2019
Terms of Use: https://www.spiedigitallibrary.org/terms-of-use

map is within 5% for all three cases. These measured results prove the robust maintenance of the surface initial forms. Our tracking of the microsurface roughness in each postprocessing state for all cases and the PSD analysis for the two SPDT workpieces demonstrated the improvement in surface quality when using the proposed technique.

Acknowledgments

This research was made possible by the Korea Basic Science Institute Foundation.

References

1. R. A. Jones, "Grinding and polishing with small tools under computer control," *Opt. Eng.* **18**(4), 184390 (1979).
2. J. H. Burge et al., "Development of optimal grinding and polishing tools for aspheric surfaces," *Proc. SPIE* **4451**, 153–164 (2001).
3. T. T. Saito, "Diamond turning of optics: the past, the present and the exciting future," *Opt. Eng.* **17**(6), 176570 (1978).
4. D. W. Kim and J. H. Burge, "Rigid conformal polishing tool using non-linear visco-elastic effect," *Opt. Express* **18**(3), 2242–2257 (2010).
5. D. D. Walker and C. R. Dunn, "Pseudo-random tool paths for CNC sub-aperture polishing and other applications," *Opt. Express* **16**, 18942–18949 (2008).
6. H. Y. Tam, H. B. Cheng, and Z. C. Dong, "Peano-like paths for sub-aperture polishing of optical aspherical surfaces," *Appl. Opt.* **52**(15), 3624–3636 (2013).
7. I. Miyamoto, "Ultra fine finishing of diamond tools by ion beams," *Precis. Eng.* **9**(2), 71–78 (1987).
8. P. Dumas et al., "Complete sub-aperture pre-polishing and finishing solution to improve speed and determinism in asphere manufacture," *Proc. SPIE* **6671**, 667111 (2007).
9. J. D. Nelson et al., "Incorporating VIBE into the precision optics manufacturing process," *Proc. SPIE* **8126**, 812613 (2011).
10. R. E. Wagner and R. R. Shannon, "Fabrication of aspherics using a mathematical model for material removal," *Appl. Opt.* **13**(7), 1683–1689 (1974).
11. X. Nie et al., "Control of mid-spatial frequency errors considering the pad groove feature in smoothing polishing process," *Appl. Opt.* **53**(28), 6332–6339 (2014).
12. T. Blalock, K. Medius, and J. D. Nelson, "Fabrication of freeform optics," *Proc. SPIE* **9575**, 95750H (2015).
13. M. Palmer, "Freeform optics fabrication and post processing," Master's Report, College of Optical Sciences, University of Arizona, Tucson, Arizona (2016).
14. Pace Technologies, "Metallographic polishing pads (PSA)," http://www.metallographic.com/Technical/Polishiing-PSA.htm (2006).

Xiangyu Guo is a graduate of the master's program at the James C. Wyant College of Optical Sciences at the University of Arizona. Her main research area focuses on the optical fabrication for freeform optics and newly developed materials like three-dimensional printing or low coefficient of thermal expansion ceramic materials. She is now a PhD candidate in the J. Mike Walker '66 Department of Mechanical Engineering, Texas A&M University.

Yong Shu is a lecturer in Aviation Maintenance NCO Academy at Air Force Engineering University. His research area covers optimization of computer controlled optical surfacing (CCOS) and utilization of different fabricating methods such as MRF, IBF, CCOS, and hydrofluoric acid etching together to improve the laser-induced damage threshold of optics.

Geon-Hee Kim is a director of the Division of Scientific Instrumentation, Korea Basic Science Institute (KBSI). He has developed various research equipment, technology, and systems, including micro-processing technology, optical measurement devices, and ultra-precision manufacturing machines. His current research interests focus on the areas of optical devices and ultra-precision manufacturing. He is a senior member of KSPE.

Michael Palmer is a graduate of the master's program at the James C. Wyant College of Optical Sciences at the University of Arizona. He is an optical and software engineering consultant and has significant experience in robotics, PID theory, optical instrumentation, fabrication, and testing.

Heejoo Choi is a postdoctoral researcher at the James C. Wyant College of Optical Sciences at the University of Arizona. He has studied the nonlinear optical harmonic generation and optical metrology. His current research mainly focuses on the development of optical metrology for science and industry.

Dae Wook Kim is an assistant professor of optical sciences and astronomy at the University of Arizona. His research area covers precision optical engineering, including interferometry and deflectometry. He is the chair of the Optical Manufacturing & Testing (SPIE) and Optical Fabrication & Testing (OSA) conferences. He is a senior member of OSA and SPIE and has been serving as an associate editor for *Optics Express*.

Downloaded From: https://www.spiedigitallibrary.org/journals/Optical-Engineering on 06 Nov 2019
Terms of Use: https://www.spiedigitallibrary.org/terms-of-use